SLAC-PUB-956
(TH)
September 1971

QUANTUM ELECTRODYNAMICS AT HIGH ENERGIES*

Hung Cheng**†
Stanford Linear Accelerator Center
Stanford University, Stanford, California 94305

Tai Tsun Wu
Gordon McKay Laboratory
Harvard University
Cambridge, Massachusetts 02138

(Reported by Hung Cheng)

To be presented at the 1971 International Symposium on Electron and Photon Interactions at High Energies, Cornell University, Ithaca, New York, August 23-27, 1971.

---

*Work supported in part by the U. S. Atomic Energy Commission

**Work supported in part by the National Science Foundation

†Permanent address: Dept. of Mathematics, Massachusetts Institute of Technology, Cambridge, Massachusetts 02139.

1. INTRODUCTION

Over the past four years, considerable efforts have been devoted to quantum electrodynamics at high energies. As a result of such intensive investigations, we have accumulated not only a wealth of knowledge on the interaction between electrons and photons at high energies, but also much basic understanding on the behavior of a high-energy particle in general. Today I would like to report on some of the most interesting developments here.

The results I shall give are therefore of two distinct kinds: (i) those which are applicable to electrons and photons only; (ii) those which are applicable to hadrons as well. The first kind includes most of the computational results on asymptotic Feynman amplitudes. To give some examples, we have now in our possession the high-energy limit of the total and the differential cross sections for (1) the Delbrück scattering process; (2) the photon-photon scattering process; (3) pair-creation process in electron-electron scattering or electron-positron scattering. Of these quantities, the pair-creation cross sections are already relevant to colliding beam experiments, as reported by Dr. Brodsky yesterday. The cross sections for Delbrück scattering are now being measured by the Lund-DESY group, while the cross sections for photon-photon scattering can probably be measured in the near future.* On the more technical side, we have developed a method (the method of impact diagrams) especially tailored to handle high-energy amplitudes, which can now be calculated very simply. The calculations we have performed are not always limited to lowest orders. One notable example is the amplitude for Delbrück scattering. In this scattering process, the charge Z of the nucleus can be so large that $Z\alpha$ is not small compared to unity. We must therefore calculate this amplitude to all orders of $Z\alpha$. This has now been done.

---

*R. W. Brown, (private communication).

Although such results are extremely interesting in themselves, much of the enthusiasm for high-energy QED was motivated by the hope that a study of the best field theory available may help us to understand high-energy scattering in general. For this purpose, we must not rely on the quantitative results of any particular Feynman diagram. Rather, we must extract the general features of all Feynman diagrams. Such a study has been carried out, and it has led to many surprising realizations on the way particles behave at high energies. It suggests that a hadron at high energies acts like a black pancake with a radius increasing logarithmically with the energy. From a theoretical viewpoint, we have now a model which embraces the droplet model, the parton model and the Regge pole model, and is completely consistent.

We shall give a systematic account of our results. We are interested only in scattering amplitudes in their high-energy limit. For the process $a+b \longrightarrow c+d$, this is defined to be the limit $s \longrightarrow \infty$, with t fixed; and for the process $a+b \longrightarrow c+d+e+\ldots$, this is defined to be the limit $s \longrightarrow \infty$, with $\vec{p}_\perp$ fixed for all outgoing particles, where the z axis is chosen to be parallel to the momenta of the incident particles (Fig. 1).

2. LOWEST-ORDER CALCULATION

Our calculation begins with the case of two-body elastic scattering processes in quantum electrodynamics. For these processes in their lowest orders, the two cases of massless photon and massive photon are so very similar that they can be treated together. For electron-electron scattering, the simplest diagram involves the exchange of one photon (Fig. 2a). At high energies, this one-photon exchange amplitude is found to be proportional to s. This is to be expected, as the scattering amplitude for exchanging a particle of spin J is always proportional to s^J. The one-photon exchange amplitude is real, as the photon is a real particle.

To get the imaginary part of the scattering amplitude, we must go to the fourth-order diagrams where two photons are exchanged (Fig. 2b). At high energies, the sum of the two-photon exchange amplitudes is imaginary and is also proportional to s, in consistency with the empirical rule of $s^{J_1+J_2-1}$ for exchanging two particles of spin J_1 and J_2, respectively. Thus, up to the fourth order, both $\lim_{s\to\infty}\frac{d\sigma}{dt}$ and $\lim_{s\to\infty}\sigma_{TOTAL}$ are finite and non-zero.

Consider next Compton scattering. Some of the diagrams for this process are shown in Fig. 3. In the first row and the first column, we show the lowest-order diagrams for Compton scattering; these diagrams are responsible for the Klein-Nishina formula. It is thus well known that the matrix element for these diagrams approaches a constant as $s\longrightarrow\infty$. That is, at high energies the matrix element is of the order e^2s^0. Next we consider radiative corrections. Their contributions to the matrix element again fail to grow as s, and are of the order e^4s^0 (with some powers of $\ell n\, s$). It is therefore natural to raise the question whether, at high energies, $d\sigma/dt\to 0$ as s^{-2} for Compton scattering. A moment's reflection indicates this is not possible. A photon is sometimes a virtual electron-positron pair; since $d\sigma/dt$ is finite and non-zero for fourth-order e-e scattering, it must be finite and non-zero for sixth-order γe scattering. The diagrams of importance are accordingly the three shown in the first row and the second column of Fig. 3, and at high energies, the sum of their contributions to the matrix element is of the order e^6s.

The lesson here is this: At high energies the importance of a diagram cannot be ascertained by merely counting its order, the asymptotic behavior of the matrix element being of great importance. We also notice that in all of the important diagrams, photons are exchanged between two groups of particles, which may be the incident particles themselves or the ones created by them. A further example of photon-photon scattering is shown in the second row of Fig. 3.

We have given[1] the high-energy behavior of all the two-body elastic scattering processes in quantum electrodynamics. The six processes studied are: (1) electron-electron scattering, (2) electron-positron scattering, (3) Coulomb scattering, (4) Delbrück scattering, (5) Compton scattering, and (6) photon-photon scattering. Some of the details of the calculations, which are extremely long, are published in the Physical Review.[2-5] We emphasize that the effect of multiphoton exchange is already treated in references 1 and 2.

3. IMPACT-FACTOR REPRESENTATION

Even with the calculations limited to the lowest non-trivial order, the high-energy behaviors of the matrix elements for the above processes are by no means simple when expressed in terms of Feynman parameters. It is therefore significant that the high-energy results for the above six processes can all be summarized in the elegant form of impact-factor representation (not to be confused with impact parameter representation). (The contributions due to one-photon exchange are not included.) The simplest form of impact-factor representation is

$$\mathcal{M}^{(ab)} \sim is(2\pi)^{-2}\int d^2 q_\perp \frac{\mathcal{I}^a\left(\vec{q}_\perp, \vec{\Delta}\right)\mathcal{I}^b\left(\vec{q}_\perp, \vec{\Delta}\right)}{\left(\left(\vec{q}_\perp + \frac{1}{2}\vec{\Delta}\right)^2 + \lambda^2\right)\left(\left(\vec{q}_\perp - \frac{1}{2}\vec{\Delta}\right)^2 + \lambda^2\right)} , \qquad (1)$$

for the process $a+b \rightarrow a+b$, where λ is the photon mass, $\frac{1}{2}\Delta+q$ and $\frac{1}{2}\Delta-q$ are the momenta of the two exchanged photons, respectively, and $\mathcal{I}^a$ and $\mathcal{I}^b$ are the impact factors for the particles a and b, respectively. A point to be emphasized is that $\mathcal{I}^a$ is independent of what particle b is, while $\mathcal{I}^b$ is independent of what particle a is. To the lowest non-trivial order, the impact factors for electron, positron, and photon are given in references 1 and 2. Slight modifications are necessary if b is a static Coulomb field or if multiphoton exchanges are taken into account.[1,2]

It is interesting to observe in (1) the following physical features: (i) The exchanged photons can carry only transverse momentum. This is evidenced by the fact that the longitudinal components of q (q_0 and q_3) do not appear in the photon propagators. (ii) As a consequence of (i), the four-momentum squared of any virtual particle remains finite as $s \to \infty$. In other words, none of the virtual particles is very far off the mass shell. (iii) The longitudinal momentum of the incident particle is always distributed in positive fractions by the particles created. For example, in the photon impact factor, we have $0 \leq \beta \leq 1$, where β and $(1-\beta)$ are, respectively, the fractional longitudinal momenta carried by the electron and the positron created by the incident photon. These three features are in fact the ones which form the basic working principles of the droplet model[6] and the parton model.[7] For example, feature (iii) is equivalent to the hypothesis of limiting fragmentation,[6] while feature (ii) is the core of Feynman's explanation of scaling in inelastic electron scattering.

From the above considerations, each of the two incident particles in a high-energy collision process can be visualized as a superposition of multi-particle virtual states. By the uncertainty principle, each virtual state can exist a finite length of time in its own center-of-mass system. By time dilation, such a virtual state can exist for a long time in any frame where it is extremely relativistic. On the other hand, in the frame of each of the incident particles, the other incident particle is Lorentz contracted into a thin slab. The particles in the two virtual states thus interact independently and simultaneously. After the interaction, the new multi-particle virtual states recombine to contribute to the scattered states. We call this physical picture the impact picture.[8] The impact picture is to be further discussed in Section 5.

If we take this physical picture as our starting point, we may construct simple rules to calculate the asymptotic form of a scattering amplitude. These rules are

graphically represented by a new kind of diagram called the impact diagram.[9,10] All of the lowest-order calculations can be reproduced almost trivially with these new rules.[9]

Since in the impact picture no special property of quantum electrodynamics is used, it is perhaps reasonable to apply the impact-factor representation to various hadronic processes. We have attempted this in the cases of inelastic scattering at high energies,[11] polarization effects,[12] and others.[13] On the more theoretical side, we have studied the relation between impact factors and form factors[9,13,14] and also apply these considerations to production processes,[15] inelastic processes,[16] and also scalar electrodynamics.[17]

Finally, we notice that the s dependence of the amplitude as given by (1) is linear. It is fun to speculate on what to expect when higher-order diagrams are taken into account. For one who is interested in the droplet model or the parton model, it would be nice if none of the terms in the scattering amplitude grow faster than s. And for one who is interested in the Regge pole model, it would be nice if the amplitude Reggeizes into

$$s^{\alpha(t)}$$

with

$$\alpha(0) = 1 ,$$

as is postulated for the Pomeranchuk trajectory.

It turns out that neither happens. What happens in quantum electrodynamics is something much more natural and satisfying than people imagined, as will be explained in the rest of this talk. Unless specified otherwise, we shall direct ourselves to the case of massive photons exclusively, since we shall be interested only in QED's possible application to hadron physics.

4. HIGHER-ORDER DIAGRAMS

A. Pionization

We shall first answer the question: Are there terms which grow faster than s as $s \to \infty$?

It is necessary to restate this question somewhat more precisely. Let us return to the three diagrams shown in the first row and second column of Fig. 3. For massless photons, the contributions to the Compton matrix element from these diagrams individually are of the order $s(\ell n\, s)^2$ or $s(\ell n\, s)^3$ in the Feynman gauge. These factors of $\ell n\, s$ greatly complicate our original calculation but are completely cancelled for $t \neq 0$. Thus, a more precise statement of the above question is as follows: Are there uncancelled terms that grow faster than s as $s \to \infty$?

This question can be restated in terms of impact diagrams.[9,10] The results of calculation with impact diagrams are of the form s multiplied by integrals which depend on t but not on s. To the lowest non-trivial orders, the integrals lead to the impact factor representation given in (1). How do the integrals behave in higher orders? If they are well-defined to all orders, we can claim a satisfactory understanding of high-energy processes. However, it turns out that the above-mentioned integrals diverge logarithmically when the orders of perturbation are those related to two-electron intermediate states in the t-channel, and the simplest example is shown in Fig. 4a. These one-loop diagrams give an uncanceled $s\, \ell n\, s$ term.

This appearance of logarithmic divergence is not a pecularity of electrodynamics, and the existence of $\ell n\, s$ has a natural physical interpretation. Let us call the sum of the longitudinal momenta of the electron-positron pair created (represented by the loop) as $\beta\omega$, where ω is the C.M. momentum of one of the incident particles. Then the divergence occurs because there is a factor $\int_0^1 \frac{d\beta}{\beta}$ in the scattering amplitude. The divergence is caused by small β, and we must cut off the lower limit of integration

at ω^{-1}. This is because when $\beta\omega$ is not large, the impact diagram method does not apply. Thus the divergence is due to the production of relatively low-energy particles in the center-of-mass system and gives in essence a factor $\ell n s$.

In cosmic-ray experiments, an excess of such low-energy pions has been observed, and is referred to as pionization.[18] Making use of this connection between $\ell n s$ and pionization, we are able to predict, on general grounds, the longitudinal momentum distribution of pionization products as follows.[19] Consider for definiteness proton-proton scattering at very high energies and let

$$\rho(p_x, p_y, p_z)\, dp_x\, dp_y\, dp_z$$

be the distribution of low-energy pions in the center-of-mass system, where both of the incoming particles move in the z-direction, then

$$\rho(p_x, p_y, p_z) = E^{-1} f(p_x, p_y) \ , \tag{2}$$

where $E = \left(p_x^2 + p_y^2 + p_z^2 + m^2\right)^{1/2}$, and $f(p_x, p_y)$ is independent of p_z but depends on p_x and p_y. We emphasize that this result (2) holds when

$$E \ll (m/M)\,\omega \ , \tag{3}$$

where ω is the energy of the incoming protons in the center-of-mass system, m is the pion mass, and M is the proton mass.

This result can be immediately generalized to multi-particle distributions. For example, for two pions

$$\rho(p_{1x}, p_{1y}, p_{1z}; p_{2x}, p_{2y}, p_{2z})$$

$$= E_1^{-1}\, E_2^{-1}\, f(E_1\, E_2 - p_{1z}\, p_{2z}; p_{1x}, p_{1y}; p_{2x}, p_{2y}) \ , \tag{4}$$

provided that both E_1 and E_2 satisfy (3). The variable $E_1\, E_2 - p_{1z}\, p_{2z}$ shows the presence of correlation between pions.

The simplest diagrams that can be used to verify (2) and (4) are those shown in Fig. 4b. It is observed that these diagrams are intimately related to "half" of the diagrams of Fig. 4a. This relation is not accidental and may be seen as follows. By the optical theorem, the imaginary part of the matrix element due to the diagrams of Fig. 4a can be found by integrating the one-particle distribution $\rho(p_x, p_y, p_z)$ from the diagrams of Fig. 4b. In particular, by (2) and (3), there is a contribution

$$\int_0^{\epsilon\omega} dp_z \int dp_x \int dp_y \, E^{-1} f(p_x, p_y) \sim \ell n(\epsilon\omega/m) \int dp_x \, dp_y \, f(p_x, p_y) = 0(\ell n s), \quad (5)$$

where ϵ is a fixed small number less than m/M. Therefore, the appearance of the factors $\ell n s$ is intimately related to pionization. We thus conclude that the appearance of $\ell n s$ is not a pecularity of electrodynamics, and may be expected also for hadron physics.

It is interesting to compare the results (2) and (4) with the parton distribution of Feynman.[7] In both cases, the invariant phase space factor $E^{-1} d^3 \vec{p}$ appears. The similarity, however, ends there. First, Feynman's formula is directed towards the off-shell parton distribution in an isolated hadron, while our result refers to the on-shell pion distribution in hadron scattering. Secondly, we remember from Eq. (4) that the two-particle distribution depends on $E_1 E_2 - p_{1z} p_{2z}$. The field-theoretic calculation from the Feynman diagram of Fig. 4b verifies this dependence, but such correlation is supposed to be absent for partons. Thirdly, an even better understanding of the difference can be obtained by comparing the diagram of Fig. 4b with the bremsstrahlung diagrams. If the analysis of the diagram of Fig. 4b is applied to the bremsstrahlung diagrams, we find the presence of low-energy particles in the C.M. system only when the mass of the emitted vector meson is zero. When this mass is not zero, ρ approaches zero rapidly for

high incident energies and hence there is no pionization. Thus pionization is entirely distinct from bremsstrahlung, and Feynman's results and ours refer to different processes.

B. One-Tower Diagrams

Next we shall answer the question: Does the amplitude Reggeize after the logarithmic factors are summed?

The lowest-order diagrams that give a contribution of the order $s(\ell n s)^n$ are those with n closed loops joined sequentially by a pair of massive photons (Fig. 5). We shall refer to these diagrams as one-tower diagrams. Therefore, for $n = 1, 2, 3, \ldots$, the coefficient of $s(\ell n s)^n$ is a power series in the fine-structure constant α, where the leading term, due to the one-tower diagrams just mentioned, is proportional to $\alpha^{2(n+1)}$. (The situation is the same for massless photons, except that there are extra factors of $\ell n s$ in the exactly forward direction, as is well known.) These one-tower diagrams are the counterparts of the ladder diagrams in ϕ^3-theory.

In the case of electron-electron scattering, these leading terms have been explicitly found[20] for all n, and are all imaginary, representing absorption. Explicitly, the sum of the n-loop tower diagrams is equal to

$$\mathcal{M}^{(n)} \sim i s \frac{(\ell n s)^n}{n!} \langle J^e, \kappa^n J^e \rangle ,$$

where κ is an operator. Summing over n, we get the amplitude

$$i \langle J^e, s^{1+\kappa} J^e \rangle \propto \frac{s^{1+a}}{(\ell n s)^2} \tag{6}$$

where

$$a = 5\alpha^2 \pi/32$$

for scalar electrodynamics,[17] and

$$a = 11\,\alpha^2\,\pi/32$$

for quantum electrodynamics.[20,21] Note that a is independent of t. This means that the tower diagrams give a fixed Regge branch point located at $J = 1 + a > 1$!

5. LIMITING BEHAVIOR OF CROSS SECTION

A. Theoretical Considerations

By the optical theorem, the sum of one-tower amplitudes gives a total cross section of the order of $s^a(\ell n\, s)^{-2}$, in violation of the Froissart bound.[22] For a while, this was to us the most puzzling paradox, but we believe that our understanding is by now fairly complete.[23]

The fact that the cross section is larger than any power of $\ell n\, s$ cannot be blamed on the process of summing only the leading terms from the one-tower diagrams. This is because the cross section for n-pair production is always positive. By choosing n sufficiently large, the corresponding n-pair production cross section is already larger than any given power of $\ell n\, s$. Thus the sum must also be larger than any power of $\ell n\, s$.

This large result $s^a/(\ell n\, s)^2$ is, however, not to be interpreted as a violation of the Froissart bound.[22] Rather, it ought to be regarded as a realization of the strongly absorptive "potential" with a coupling constant increasing with energy, as conceived in Froissart's original paper.[22] Thus, in a two-particle scattering process, if the interaction takes place at a sufficiently close transverse distance from the center of the target, the incident particle creates slow particles in the C.M. system and is lost to the beam. If the transverse distance involved is large, the incident particle does not necessarily create pionization products and may survive. Mathematically, this can be achieved by including not only the one-tower

diagram but also all of the multi-tower diagrams illustrated in Fig. 6. Summing over the leading terms from all of these diagrams, we obtain the fermion-fermion elastic scattering amplitude as[24]

$$\frac{1}{2} i m^{-2} s \, \delta_{12} \, \delta_{1'2'} \int d\vec{x}_\perp \, e^{i\vec{\Delta}\cdot\vec{x}_\perp}\left(1 - e^{-A}\right) \quad . \tag{7}$$

In (7), m is the mass of the fermion, δ_{12} and $\delta_{1'2'}$ are the Kronecker delta of the spins, $\vec{\Delta}$ is the momentum transfer, and A is related to the Fourier transform of the asymptotic amplitude due to the sum of one-tower diagrams. Specifically, if we expand $\left(1 - e^{-A}\right)$ in (7) into a Taylor series in A, the term in (7) proportional to A is the high-energy amplitude due to the sum of the one-tower diagrams. In fact, the A^N term in (7) is the high-energy amplitude for the sum of the N-tower diagrams.

In the limit $s \longrightarrow \infty$ and $\left|\vec{x}_\perp\right| = 0(\ell n s)$, we have[23]

$$A \sim b s^a \, e^{-\mu\left|\vec{x}_\perp\right|} (\ell n s)^{-2} \quad , \tag{8}$$

where b and μ are real constants. In fact, $\mu < 2\lambda$, where λ is the mass of the vector meson. With (7) and (8), the Froissart bound is saturated but not violated.

The inclusion of multi-tower diagrams may appear somewhat arbitrary. Furthermore, we know that the exponentiation form (7), with A related to the one-tower diagrams, is valid in the leading order of α but not in the next leading order.[24] Physically, the exponentiation form (7) is valid only if the incident particle is treated as a point particle with no structure or internal degrees of freedom.[25-28] Fortunately, for the purpose of obtaining the asymptotic form of the scattering amplitude, the validity of (7) is not crucial.

Let us, instead of (7), express the scattering amplitude in the impact-distance representation

$$\mathcal{M}(s,t) \sim \frac{1}{2} i\, m^{-2}\, s \int d\vec{x}_\perp e^{i\vec{\Delta}\cdot\vec{x}_\perp} S(s,\vec{x}_\perp) \quad ,$$

where $\mathcal{M}(s,t)$ includes the contribution of all diagrams in the world. Then the function $S(s,\vec{x}_\perp)$ is the opacity at the distance and energy at which it is evaluated. By a Fourier transform, we get

$$S(s,\vec{x}_\perp) = -2 i s^{-1} m^2 \int \frac{d^2\Delta}{(2\pi)^2} e^{-i\vec{\Delta}\cdot\vec{x}_\perp} \mathcal{M}(s,-\Delta^2) \quad . \tag{9}$$

We shall consider the equation above in the limit $|\vec{x}_\perp| \longrightarrow \infty$.

It is important to realize that, if we replace $\mathcal{M}(s,-\Delta^2)$ by $(t-\lambda^2)^{-1}$ in the equation above, $S(s,\vec{x}_\perp)$ would be asymptotically proportional to $e^{-\lambda|\vec{x}_\perp|}$. Because of this exponential decrease, the diagrams with higher thresholds in the t-channel are expected to contribute less to $S(s,\vec{x}_\perp)$ for large $|\vec{x}_\perp|$. Thus the important diagrams are those with two-vector meson cuts in the t-channel. The one-tower diagrams are the leading diagrams of this kind, and the inclusion of other diagrams of this kind merely modifies the kernel κ in Eq. (6). We therefore conclude that $S(s,\vec{x}_\perp)$ is given by the one-tower diagrams, or the right side of (8), when $|\vec{x}_\perp|$ is sufficiently large, although the constants a, b, and μ should be modified if the coupling is strong. If we now fix $|\vec{x}_\perp|$ and increase s, the right side of (8) increases. This means that the interaction extends into larger and larger transverse distances as the energy increases. When the energy is sufficiently high or the transverse distance is not large enough, the right side of (8) becomes appreciable, and we may no longer approximate $S(s,\vec{x}_\perp)$ by the one-tower diagrams.

This merely says that when scattering is appreciable, we must take rescattering into account, and multi-tower diagrams, as well as others, must be included. This happens when the right side of (8) becomes of the order of unity or

$$|\vec{x}_\perp| \leq R = R_0 \ell n s \ , \tag{10}$$

where

$$R_0 = a/\mu \ . \tag{11}$$

From the above considerations, we conclude that, at extremely high energies, a particle acts like a Lorentz contracted pancake which can be roughly separated into two regions: (i) A black core with a radius R given in (10) which expands logarithmically with the energy. In this core, the right side of (8) is much larger than one and the absorption is almost complete. (ii) A gray fringe with a width 0(1). In the gray fringe, the right side of (8) is of the order of one and the absorption is partial. This is schematically illustrated in Fig. 7 and, together with the physical picture discussed in Section 3, forms a complete description of the impact picture.

B. Experimental Predictions of Elastic Scattering

Many experimental predictions of hadron-hadron scattering follow directly from the impact picture. These predictions mark a drastic departure from current concepts. It will be interesting to see if they will pass the test of experiments which will be performed at the National Accelerator Laboratory or at the Intersecting Storage Ring at CERN.

Let us derive the asymptotic form of the elastic scattering amplitude. In the first approximation, we may put

$$S(s,x) = \begin{cases} 1 \ , & |\vec{x}_\perp| < R \ , \\ 0 \ , & |\vec{x}_\perp| > R \ . \end{cases} \tag{12}$$

In other words, we shall include the contribution of the black core only. Then we have

$$\mathcal{M}(s,t) \sim \frac{1}{2} i m^{-2} s \int_{|\vec{x}_\perp| < R} d\vec{x}_\perp e^{i\vec{\Delta}\cdot\vec{x}_\perp}$$

$$= i\pi m^{-2} s \Delta^{-1} R J_1(\Delta R) . \tag{13}$$

At the forward direction $\Delta = 0$, (13) is equal to

$$\frac{1}{2} i\pi m^{-2} R_0^2 s (\ell n s)^2 . \tag{14}$$

And if $\Delta R \gg 1$, (13) becomes

$$i m^{-2} s \sqrt{\frac{2\pi R}{\Delta^3}} \cos\left(\Delta R - \frac{3}{4}\pi\right)$$

$$= -\frac{1}{2} i m^{-2} s \sqrt{\frac{\pi R_0 \ell n s}{\Delta^3}} \left[(1+i) s^{i\Delta R_0} + (1-i) s^{-i\Delta R_0}\right] . \tag{15}$$

From (14) and the optical theorem, we have

$$\sigma_{TOTAL} = 2\pi R_0^2 (\ell n s)^2 + 0(R) , \tag{16}$$

which rises indefinitely with energy. From (13), we get

$$\frac{d\sigma_{ELASTIC}}{dt} \sim \frac{\pi R_0^2}{\Delta^2} (\ell n s)^2 J_1^2 (\Delta R_0 \ell n s) \tag{17}$$

Thus the usual diffraction peak is expected for the elastic scattering amplitude around the forward direction. Furthermore, let Γ be the value of $-t$ at which

the first dip occurs, then

$$\Gamma\sigma_{\text{TOTAL}} = 2\pi^3 \beta_1^2 + 0\,(R^{-1})\,, \tag{18}$$

where $\beta_1 = 1.2197$ is the first zero of $J_1(\beta\pi)$. Numerically

$$2\pi^3\beta_1^2 = 35.92\ \text{mb}\ (\text{BeV/c})^2\,. \tag{19}$$

We also have

$$\sigma_{\text{ELASTIC}} = \pi R_0^2\,(\ell n s)^2 + 0\,(R) \tag{20}$$

and hence

$$\frac{\sigma_{\text{ELASTIC}}}{\sigma_{\text{TOTAL}}} = \frac{1}{2} + 0\,(R^{-1})\,. \tag{21}$$

C. Experimental Predictions of Inelastic Scattering

The impact picture has direct experimental consequences on diffractive inelastic processes also.[29] By a diffractive process, we mean one in which the exchange has the quantum numbers of a vacuum trajectory ("Pomeron"). Thus our considerations apply, for example, to the spin-flip amplitude for $p+p \to p+p$ and the amplitudes for $\pi+p \to \pi+p^*(1470)$, $p+p \to p+p+\pi^+ +\pi^-$ and $\gamma + p \to \rho + p$.

Consider a scattering problem with N channels which are coupled through diffractive processes. For example, we may imagine that we are dealing with the problem $p+p \to p+p$ with the channels representing the various helicity states of the protons. Let the scattering matrix be written in the impact distance representation

$$\frac{1}{2} i m^{-2} s \int d\vec{x}\ e^{i\vec{\Delta}\cdot\vec{x}_\perp} \left[I + a(\vec{x}_\perp)\right]\,, \tag{22}$$

where $a(\vec{x}_\perp)$ is an NxN matrix which may be dependent on energy as well as other kinematic variables and I is the unit matrix.

It is important to recognize that, since all diffractive processes are mediated by the same Pomeron, the effective "potential" involved has the same range and the same energy dependence. In other words, a diffractive inelastic process is motivated by the same exchanges as those in an elastic process. The matrix $a(\vec{x}_\perp)$ describes the scattering mediated by such exchanges (with its diagonal matrix elements representing elastic processes). Thus all of the matrix elements of $a(\vec{x}_\perp)$, diagonal or off-diagonal, must be of the same order of magnitude. Since the very words "black core" mean that the diagonal matrix elements of $a(\vec{x}_\perp)$ are small there, the off-diagonal matrix elements of $a(\vec{x}_\perp)$ must also be small there. Thus we conclude that

$$a_{ij}(\vec{x}_\perp) \sim 0 , \qquad i, j = 1, 2, \ldots\ldots N , \tag{23}$$

inside the black core.

Outside of the black core, there is a gray fringe of thickness 0(1). The area of this gray fringe is therefore of the order of $\ell n s$. By definition, the diagonal matrix elements of $a(\vec{x}_\perp)$ in the gray fringe are 0(1). Thus all matrix elements of $a(\vec{x}_\perp)$ are 0(1) there. We therefore have, inside the gray fringe,

$$a_{ij}(\vec{x}_\perp) = 0(1) , \qquad i, j = 1, 2, \ldots\ldots N . \tag{24}$$

From (22), (23), and (24), we see that, while the dominant contribution to an elastic process comes from the black core, the dominant contribution to a diffractive inelastic process comes from the gray fringe. (Remember that the unit matrix I is diagonal.) Furthermore, since $a(\vec{x}_\perp)$ is of the order of unity in the gray fringe, the integrated cross section for a diffractive inelastic process is of the order of the area of the gray fringe, and hence is of the order of $\ell n s$. Thus

for hadron-hadron scattering, the total cross section for an inelastic diffractive process is asymptotically

$$\sigma_{\text{diff}} = C R + 0(1) , \tag{25}$$

where C is a constant that is independent of energy but dependent on the diffractive process under consideration; if neither spin nor parity is exchanged, the scattering amplitude is proportional to

$$R J_0(R\Delta) \tag{26}$$

near the forward direction, where Δ is the momentum transfer; and in particular it follows from (26) that

$$\Gamma' \sigma_{\text{tot}} = 14.15 \text{ mb } (\text{GeV}/c)^2 + 0(R^{-1}) , \tag{27}$$

where Γ' is the value of $-t = \Delta^2$ at which the first dip occurs.

The considerations are slightly different for a photoproduction process. This is because, to a bare photon, the proton is not black but transparent as far as strong interaction is concerned. A real photon is a superposition of a bare photon state and hadron states. Thus the proton looks like an expanding gray disk to the real photon. Since the core is not black, a diffractive inelastic process can occur inside this disk. This means that the cross section for photo ρ production is of the order of $(\ell n s)^2$. In a diffractive photoproduction process, then, the total cross section is asymptotically

$$\sigma_{\text{photo}} = C' \alpha R^2 + 0(R) , \tag{28}$$

where C' is a constant just like C, and α is the fine-structure constant; and if neither spin nor parity is exchanged, the scattering amplitude is proportional to

$$R \Delta^{-1} J_1 (R\Delta) , \tag{29}$$

identical to that for elastic hadron-hadron processes.

It is extremely interesting to ponder as to whether the considerations above in fact hold for hadron-hadron scattering as well—that is, whether a hadron at high energies behaves like a gray disk rather than like a black disk with gray fringe.

We conclude the study on inelastic scattering with a few remarks.

1. The discussions above can be extended to processes involving Regge exchange with quantum numbers. We first observe that the exchange of a Regge pole is difficult to occur in the black core. This is because, if the incident particles are separated by a transverse distance less than the radius of the black core, it is almost impossible to have an exclusive exchange process (i.e., without the additional production of particles). As a result, a Regge exchange process is limited to the region that is not very black. Mathematically, the amplitude for the exchange process is given by

$$\int d\vec{x}_\perp \left[S(s,\vec{x}_\perp) - 1\right] B(s,\vec{x}_\perp) \ , \tag{30}$$

where B is the Fourier transform of the Regge-pole term for the exchange. Since $B(s,\vec{x}_\perp)$ vanishes exponentially as $|\vec{x}_\perp| \longrightarrow \infty$, the conventional Regge pole term must be modified to a reduced value as the black core expands.

2. The considerations can also be applied to pionization processes. For example, the integrated cross section for the process $e^- + e^- \longrightarrow e^- + e^- + e^+ + e^-$, with the created pair having energies 0(1) in the center-of-mass system, is of the order of $(\ell n\, s)^{-3/2}$, which decreases with energy.[29]

Field theoretic models in support of the conclusions in this section can be found elsewhere[29] and we shall not elaborate on them here.

D. The Generalized Impact Factor Representation

Finally, we collect some formulae here for the amusement of those theorists who are interested in multi-tower exchanges.

For elastic e - e scattering, the sum of the leading terms of all multi-tower amplitudes is given by (7).

For elastic e - γ scattering, the sum of the leading terms of all multi-tower amplitudes is given by

$$\mathcal{M}^{(e\gamma)} \sim \frac{1}{2} i s \int d\vec{x}_\perp \, d\vec{y}_\perp \, I^\gamma(\vec{\Delta}, \vec{y}_\perp) \, I^e_{12} \exp(i\vec{\Delta}\cdot\vec{x}_\perp) \left\{1 - \exp\left[-A(s, \vec{x}_\perp, \vec{y}_\perp)\right]\right\}. \quad (31)$$

In (31), $I^\gamma(\vec{\Delta}, \vec{y}_\perp)$ is the photon impact factor in the position space, $I^e_{12} = \frac{e^2}{m} \delta_{12}$, and $A(s, \vec{x}_\perp, \vec{y}_\perp)$ is a gauge-invariant function given explicitly elsewhere.[30]

For elastic γ - γ scattering, the sum of the leading terms of all multi-tower amplitudes is given by

$$\mathcal{M}^{(\gamma\gamma)} \sim \frac{1}{2} i s \int d\vec{x}_\perp \, d\vec{y}_\perp \, d\vec{y}_\perp' \, I^\gamma(\vec{\Delta}, \vec{y}_\perp) I^\gamma(\vec{\Delta}, \vec{y}_\perp') \exp(i\vec{\Delta}\cdot\vec{x}_\perp)$$

$$\left\{1 - \exp\left[-A(s, \vec{x}_\perp, \vec{y}_\perp, \vec{y}_\perp')\right]\right\}, \quad (32)$$

where $A(s, \vec{x}_\perp, \vec{y}_\perp, \vec{y}_\perp')$ is a gauge invariant function also given in reference 30.

6. SUMMARY

Quantum electrodynamics has successfully explained the interaction of photons and electrons. It is the only relativistic field theory which produced for us both theoretical and experimental triumphs in the past. Today, seeking the answer to the mystery of high-energy scattering, we once again look into quantum electrodynamics, and it has once again responded. It has shown us a most natural way to realize the near constancy of the total cross section, and it has taught us the ways a particle with high energies behaves. The solution it provides satisfies all honored physical principles such as unitarity, dispersion relation, and crossing symmetry. We ask: Is this solution relevant to hadron-hadron scattering?

The test will and must come from experiments. It is, nevertheless, worthwhile to make a critical appraisal here of what we have done.

We have shown that, in quantum electrodynamics with massive photons, the Froissart bound is almost saturated (the cross section is, more precisely, $\left[\ell n \frac{s^a}{(\ell n s)^2}\right]^2$). A summary of the arguments leading to this conclusion is: (i) one-tower diagrams give a cross section increasing as a power of s; (ii) this implies that the interaction extends into logarithmically large transverse distances; (iii) the cross section therefore rises logarithmically.

As we have explained in Section 5A, (i) is certainly correct. The correctness of (ii) depends on whether there are diagrams (in addition to the one-tower diagrams) which also contribute significantly at large transverse distances and cancel the contribution from the one-tower diagrams. These diagrams, if they exist, must have two-photon cuts in the t-channel, and they may add up to give an amplitude of the order of s^{1+b}. However, b is, at most, of the order of α^3, and, at least for sufficiently small α, should be small compared to a, as given in the equations below (5). Thus (ii) is most likely to be true in quantum electrodynamics.

If (ii) is true, then (iii) automatically follows unless the absorption at fixed transverse distances decreases as the energy increases. Since we expect more channels to open up at higher energies, it is difficult to visualize how such a phenomenon can occur. It is therefore likely that (iii) is true also. The proof for the near-saturation of the Froissart bound in QED with massive photons is therefore reasonable, if not entirely mathematically rigorous.

Is the near-saturation of the Froissart bound a peculiarity of QED? To answer this question, we observe that, of (i), (ii), and (iii), only (i) is a special result of QED. To see how (i) should be modified in other field theories, let us, to be definite, consider ϕ^3-theory, where the counterparts of one-tower diagrams are ladder diagrams. It is well known that ladder diagrams give the amplitude $\beta(t)s^{\alpha(t)}$. We then have three possibilities: (a) $\alpha(0) > 1$; (b) $\alpha(0) < 1$; (c) $\alpha(0) = 1$. If (a) is true, then we would have the equivalent of (i) and the near-saturation of Froissart bound is also realized in ϕ^3-theory. If (b) is true, then $\alpha(0)$ of the Pomeranchuk trajectory must be very close to one, and the near constancy of the total cross section must be explained as an accident. For lack of dynamical reasons, (c) can be true only by a miracle. (On the other hand, it can be shown that, as long as the coupling is strong enough, (a) is always true.[31])

The arguments above can, of course, be extended to other field theories. They are probably even independent of the validity of any field theories. The necessary requirement for the realization of near-saturation of the Froissart bound is that the sum of all amplitudes from ladder-like diagrams (or, more generally, the part of the scattering amplitude with the lowest t-cut) gives an amplitude $\beta(t)s^{\alpha(t)}(\ell ns)^{\gamma(t)}$ with $\alpha(0) > 1$. This is perhaps likely to happen for sufficiently strong coupling.

If $\alpha(0) > 1$, then the Pomeron identified with $\alpha(t)$ is a singularity (either a pole or a branch point) in the J-plane located at $J > 1$ when $t = 0$. In

this case, the amplitude for one-Pomeron exchange, being proportional to $s^{\alpha(0)}$ at $t = 0$, violates the Froissart bound. The amplitude for n-Pomeron exchange, being proportional to $s^{n\alpha(0)-n+1}$ at $t = 0$, is even larger. However, these terms cancel themselves and the sum is given by (13) or (15). We see from (15) that regardless of whether the Pomeron is a branch point or a pole, the leading singularities of the scattering amplitude in the J-plane are always two moving branch points; for $t < 0$, these branch points form complex conjugate pairs on the line $\mathrm{Re}\, J = 1$; at $t = 0$, both reach the point $J = 1$; at $t > 0$, they move on the real J-axis—one to the right and the other to the left. This is schematically plotted in Fig. 8.

In closing, we recall that, in 1959, Regge first showed that the scattering amplitude in potential scattering is asymptotically of the form $\beta(t)\, s^{\alpha(t)}$ as $s \longrightarrow \infty$.[32] This form was immediately assumed to hold for the scattering amplitude in relativistic processes.[33-36] Such an assumption is entirely arbitrary, and it is probably time to make a re-examination of this assumption.

In potential scattering, the amplitude in the high-energy limit is dominated by Regge poles, which are related to the resonances and bound states of the crossed channel. In relativistic scattering, the amplitude for ladder-like diagrams is also dominated by Regge poles, and these Regge poles are also responsible for the resonances and bound states of the crossed channel. This suggests that the analogue of the potential theory results holds for the amplitude of ladder-like diagrams alone, not the entire scattering amplitude itself. In fact, the Born series of the scattering amplitude in potential scattering is identical to the amplitudes of ladder diagrams in ϕ^3-theory, if one of the masses of the particles is set to infinity in the latter case.

The amplitude for potential scattering is not required to satisfy the unitarity condition in the s-channel, and there is no restriction on $\alpha(0)$. By the same token, the amplitude for the ladder-like diagrams is not required to satisfy the unitarity condition in the s-channel, and it is unnatural to set the restriction $\alpha(0) \leq 1$. In the relativistic case, unitarity in the s-channel for the complete scattering amplitude is always insured by the existence of diagrams such as the multi-Reggeon exchange diagrams, which have no meaning in the potential case. The restriction $\alpha(0) \leq 1$ is therefore also unnecessary.

If $\alpha(0) \leq 1$, it makes no difference whether we adopt the old or the new analogue. Then, of course, $\alpha(0)$ must be either equal to, or very close to, unity. One may wonder why it is so, and as of now there is no dynamical explanation. Perhaps, however, the coupling constants in hadron-hadron scattering are so strong that $\alpha(0) > 1$. Then, no matter what value $\alpha(0)$ takes, the total cross section is very nearly a constant. Perhaps this is the way nature works. We must wait for the verdict of future experiments.

References and Footnotes

1. H. Cheng and T. T. Wu, Phys. Rev. Letters, 22, 666 (1969).
2. H. Cheng and T. T. Wu, Phys. Rev. 182, 1852 (1969).
3. H. Cheng and T. T. Wu, Phys. Rev. 182, 1868 (1969).
4. H. Cheng and T. T. Wu, Phys. Rev. 182, 1873 (1969).
5. H. Cheng and T. T. Wu, Phys. Rev. 182, 1899 (1969).
6. C. N. Yang in Proceedings of the Third Topical Conference on High Energy Collisions of Hadrons, Stony Brook, New York (1969), and the references cited therein.
7. R. Feynman, Phys. Rev. Letters 23, 1415 (1969).
8. H. Cheng and T. T. Wu, Phys. Rev. Letters 23, 670 (1969).
9. H. Cheng and T. T. Wu, Phys. Rev. D1, 1069 (1970).
10. H. Cheng and T. T. Wu, Phys. Rev. D1, 1083 (1970).
11. H. Cheng and T. T. Wu, Phys. Rev. Letters 22, 1409 (1969); and Phys. Rev. 183, 1324 (1969).
12. H. Cheng and T. T. Wu, Phys. Rev. Letters 23, 351 (1969).
13. H. Cheng and T. T. Wu in Proceedings of the Third Topical Conference on High Energy Collisions of Hadrons, Stony Brook, New York (1969).
14. H. Cheng and T. T. Wu, Phys. Rev. 184, 1868 (1969).
15. H. Cheng and T. T. Wu, Phys. Rev. D1, 456 (1970).
16. H. Cheng and T. T. Wu, Phys. Rev. D1, 459 (1970). There are a number of mistakes in this paper in regard to the longitudinal axial vector meson.
17. H. Cheng and T. T. Wu, Phys. Rev. D1, 467 (1970).
18. See, for example, Proceedings of the Tenth International Conference on Cosmic Rays, Calgary, Canada, 1967 (Canadian J. Phys. 46S (1968)). The rapporteur paper of M. Koshiba at this conference is especially illuminating

but unfortunately not published. See also M. Koshiba in High-Energy Collisions, ed. by C. N. Yang et al. (Gordon and Breach Science Publishers, Inc., New York, 1969).

19. H. Cheng and T. T. Wu, Phys. Rev. Letters 23, 1311 (1969).
20. H. Cheng and T. T. Wu, Phys. Rev. D1, 2775 (1970).
21. G. V. Frolov, V. N. Gribov and L. N. Lipatov, Phys. Letters 31B, 34 (1970).
22. M. Froissart, Phys. Rev. 123, 1053 (1961).
23. H. Cheng and T. T. Wu, Phys. Rev. Letters 24, 1456 (1970).
24. H. Cheng and T. T. Wu, Phys. Rev. 186, 1611 (1969).
25. I. J. Muzinich, G. Tiktopoulous, and S. B. Treiman, Phys. Rev. D3, 1041 (1971).
26. H. Cheng and T. T. Wu, Phys. Rev. D3, 2377 (1971).
27. H. Cheng and T. T. Wu, Phys. Rev. D3, 2394 (1971).
28. H. Cheng and T. T. Wu, High-Energy Scattering in ϕ^3-Theory and the Breakdown of Eikonal Approximation, I and II, (DESY Report 71/13 and 71/16).
29. H. Cheng and T. T. Wu, Diffractive Inelastic Processes at Extremely High Energies, Phys. Letters (submitted for publication).
30. H. Cheng and T. T. Wu, The Impact Factor Representation (Unpublished).
31. H. Cheng and T. T. Wu, Regge Poles for Large Coupling Constants II, DESY report 71/31 (1971).
32. T. Regge, Nuovo Cimento 14, 951 (1959).
33. G. F. Chew and S. C. Frautschi, Phys. Rev. Letters 7, 394 (1961).
34. R. Blankenbecler and M. L. Goldberger, Phys. Rev. 126, 766 (1962).
35. S. C. Frautschi, M. Gell-Mann and F. Zachariasen, Phys. Rev. 126, 2204 (1962).
36. For a more recent review, see H. M. Chan in The Fourteenth International Conference on High-Energy Physics, Vienna, 1968 (CERN, Geneva, 1968).

Figure Captions

Fig. 1. Definition of the high-energy limit.

Fig. 2. (a) Diagram of one-photon exchange in electron-electron scattering.

(b) Diagrams of two-photon exchange in electron-electron scattering.

Fig. 3. Orders of magnitude for various Feynman diagrams.

Fig. 4. (a) Lowest-order diagrams that contribute an uncanceled term $s \ell n s$ to the scattering amplitude.

(b) Lowest-order diagrams for pionization.

Fig. 5. Example of a one-tower diagram.

Fig. 6. Example of a multi-tower diagram.

Fig. 7. Schematic plot of the appearance of a high-energy particle.

Fig. 8. The singularities for the complete scattering amplitude in the complex J-plane.

Collaborator: Prof. T. T. Wu, Harvard University

$a+b \longrightarrow c+d$

$s \longrightarrow \infty$

t Fixed

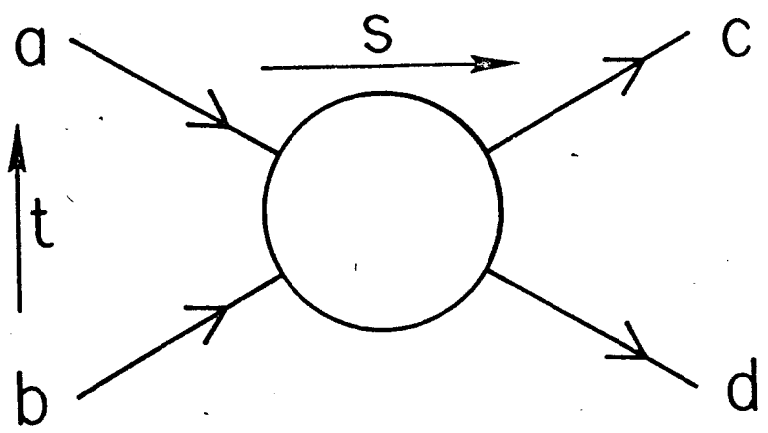

$a+b \longrightarrow c+d+e+\cdots$

$s \longrightarrow \infty$

$\vec{p}_\perp$ Fixed for all outgoing particles

1960A8

Fig. 1

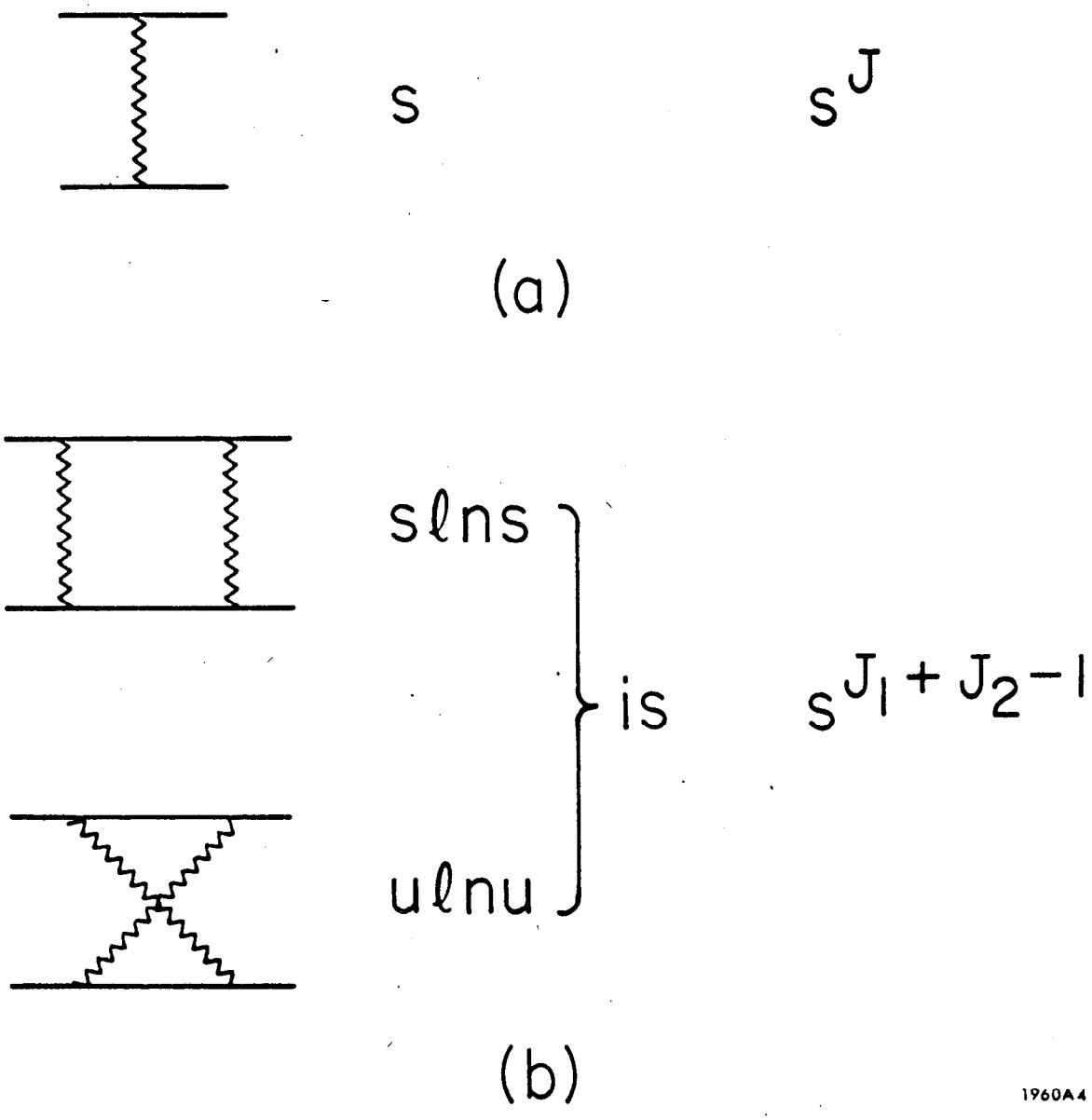

Fig. 2

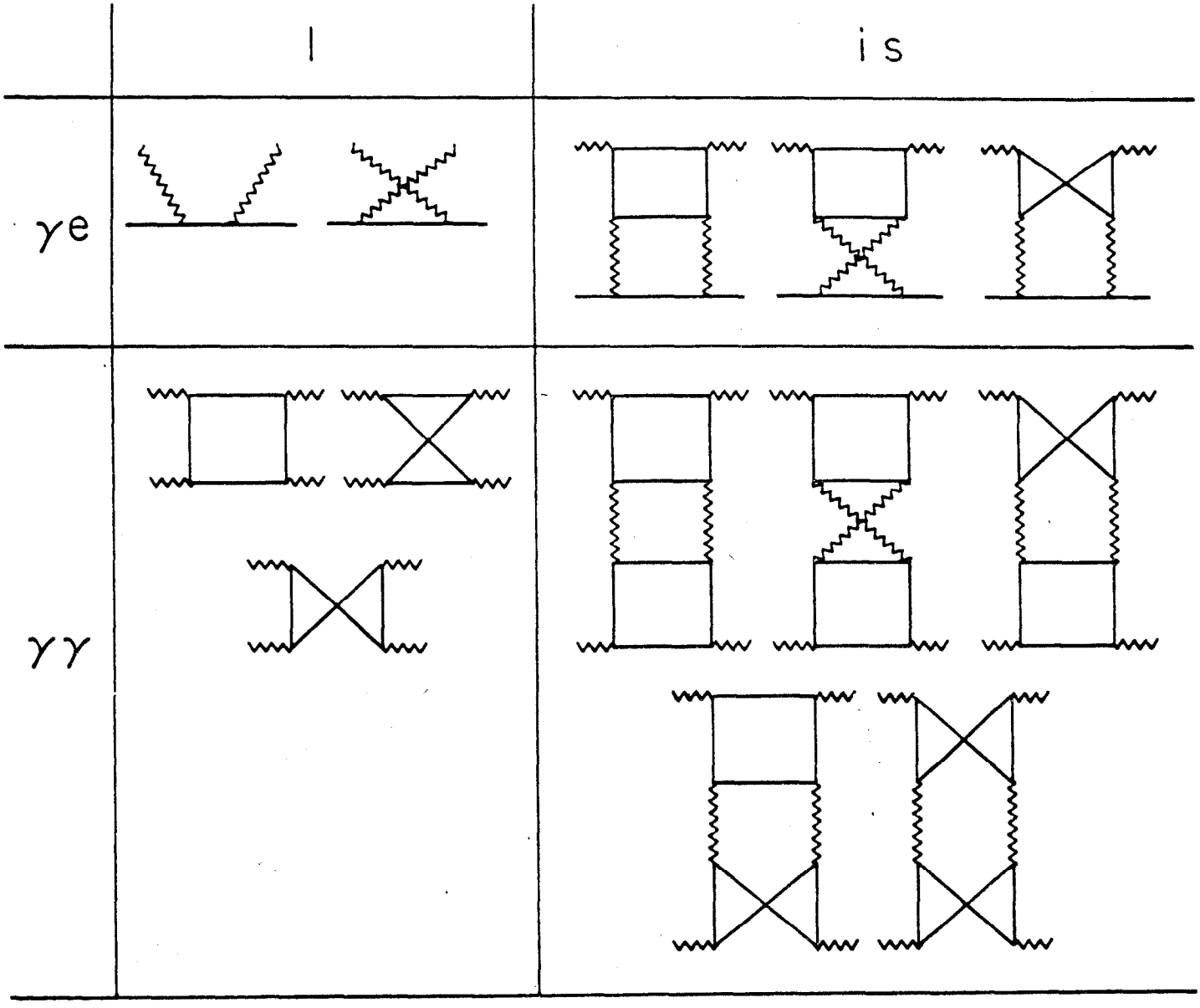

$$a + b \rightarrow c + d$$

$$\mathcal{M} \sim is \int \frac{d^2 q_\perp}{(2\pi)^2} \frac{\mathcal{I}^{ac}\left(\vec{\Delta}, \vec{q}_\perp\right) \mathcal{I}^{bd}\left(\vec{\Delta}, \vec{q}_\perp\right)}{\left[\left(\frac{1}{2}\vec{\Delta} + \vec{q}_\perp\right)^2 + \lambda^2\right]\left[\left(\frac{1}{2}\vec{\Delta} - \vec{q}_\perp\right)^2 + \lambda^2\right]}$$

1960A6

Fig. 3

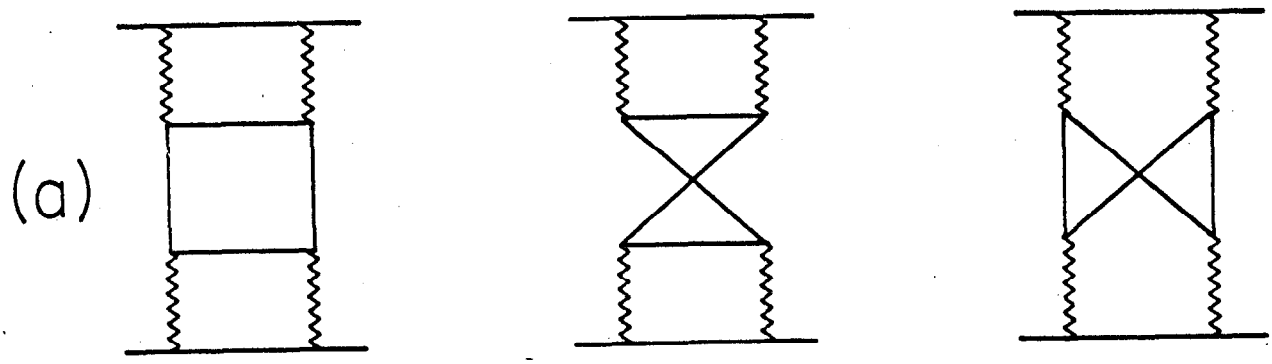

$is\ell ns\mathcal{K}$

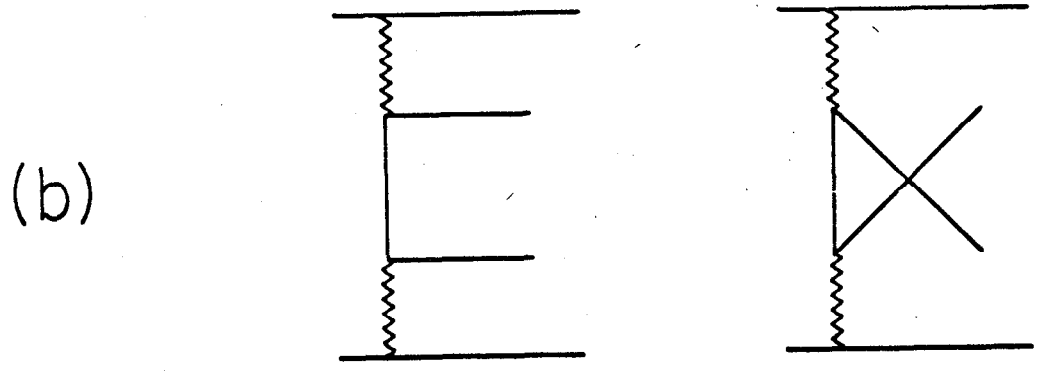

$$\int_{\omega^{-1}}^{1} \frac{dx}{x} = \ell n\omega$$

1960A5

Fig. 4

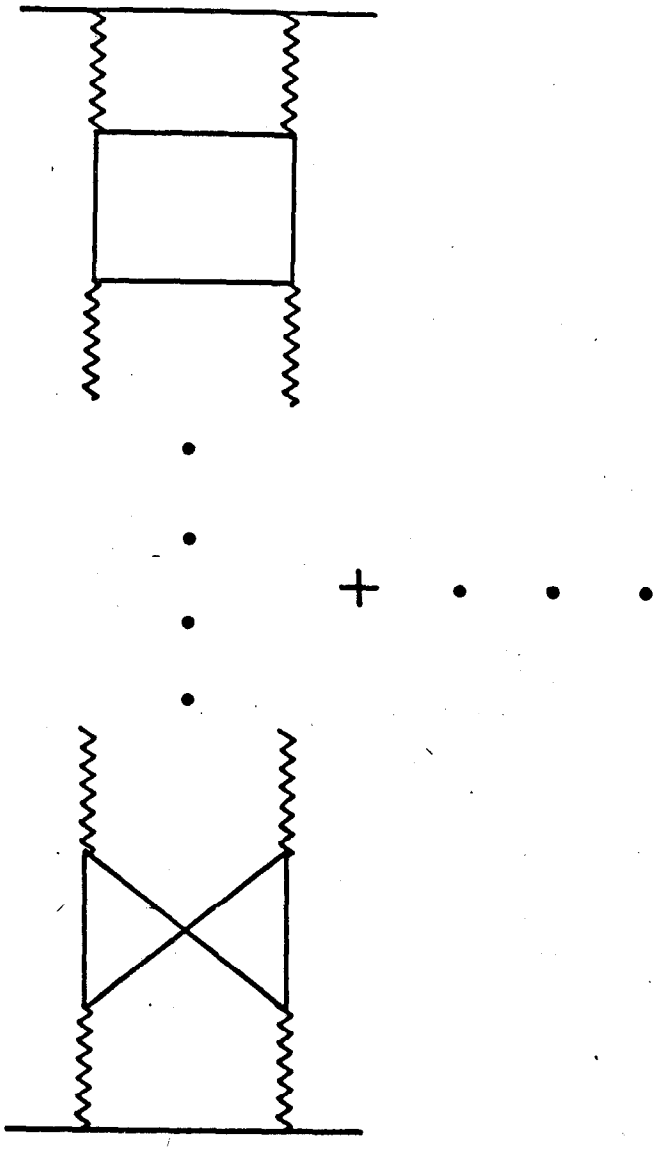

$$\mathcal{M}^{(n)} \sim is \frac{(\ell n\, s)^n}{n!} \langle J^e, \kappa^n J^e \rangle$$

$$\Sigma \mathcal{M}^{(n)} \sim i \langle J^e, s^{1+\kappa} J^e \rangle \propto \frac{is^{1+a}}{(\ell n\, s)^2}$$

$$a = \frac{11 \alpha^2 \pi}{32}$$

1960A9

Fig. 5

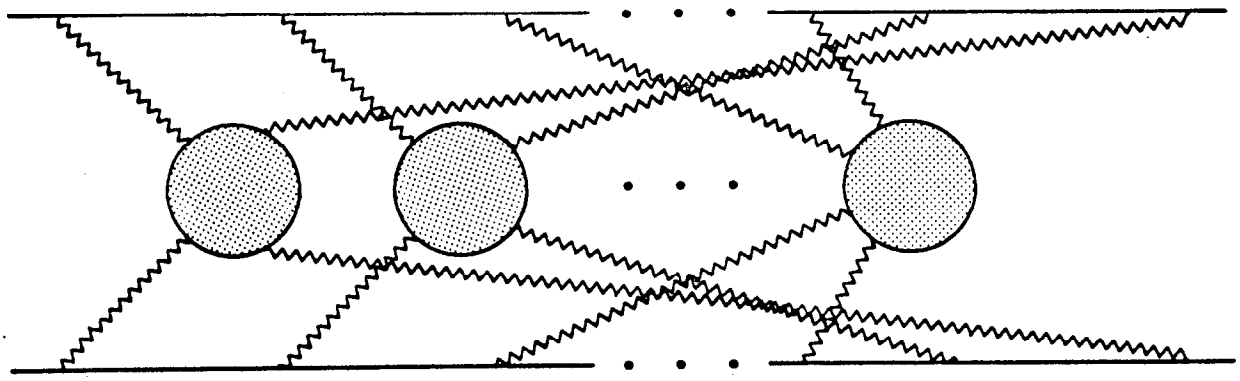

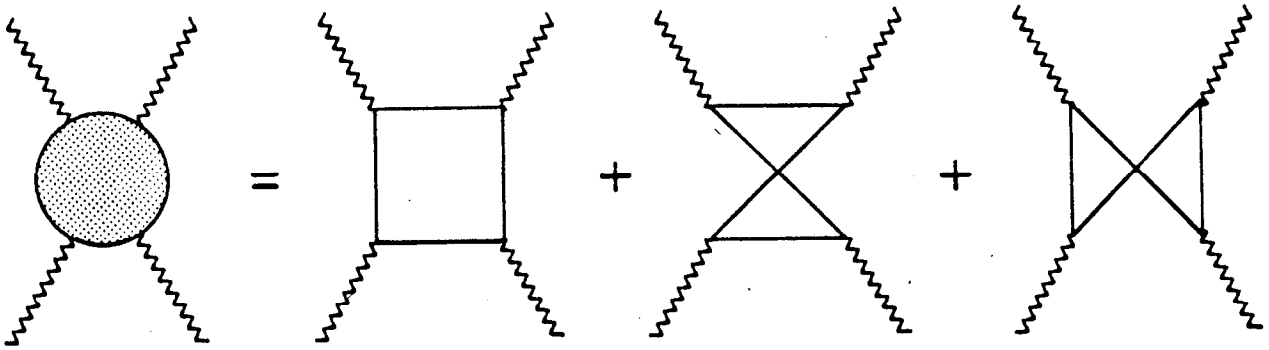

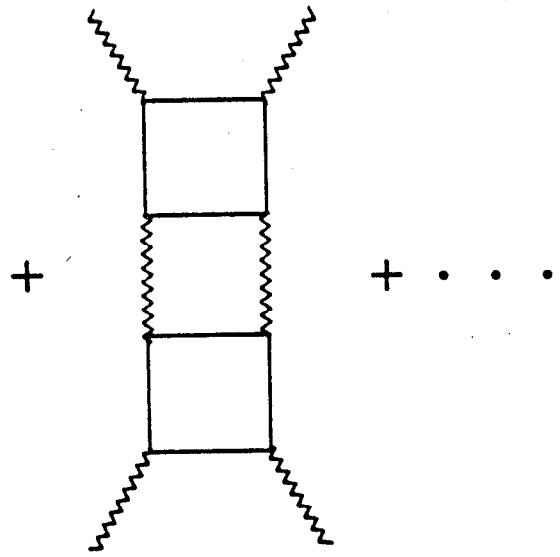

1960A3

Fig. 6

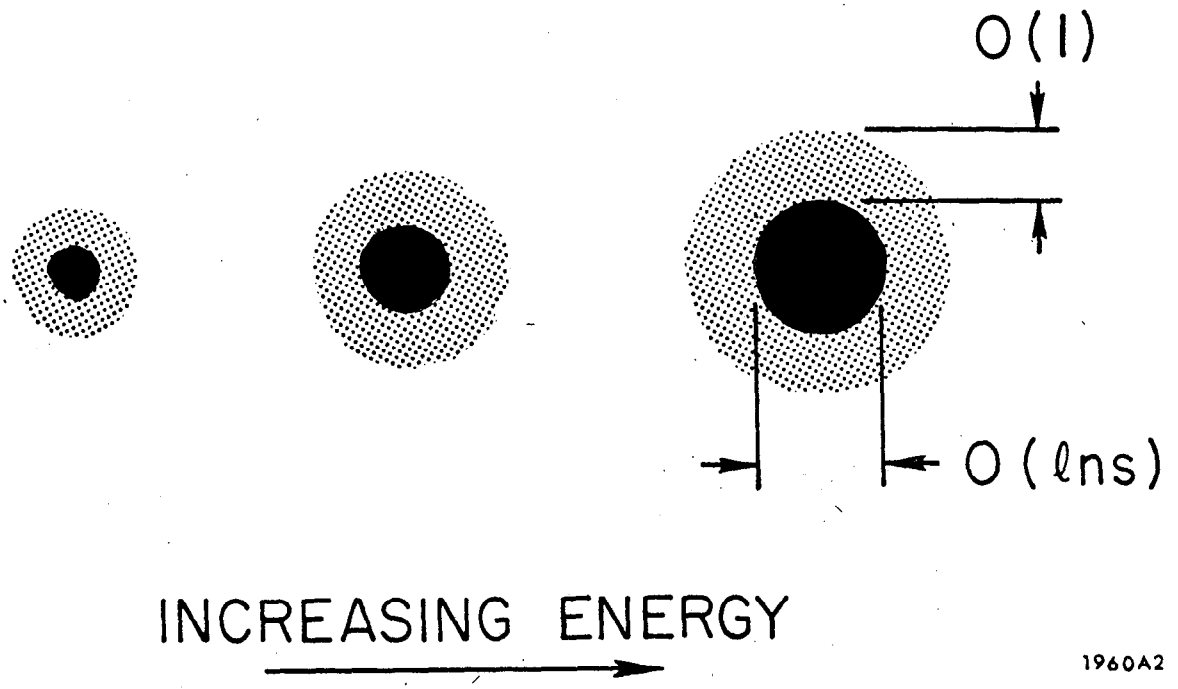

Fig. 7

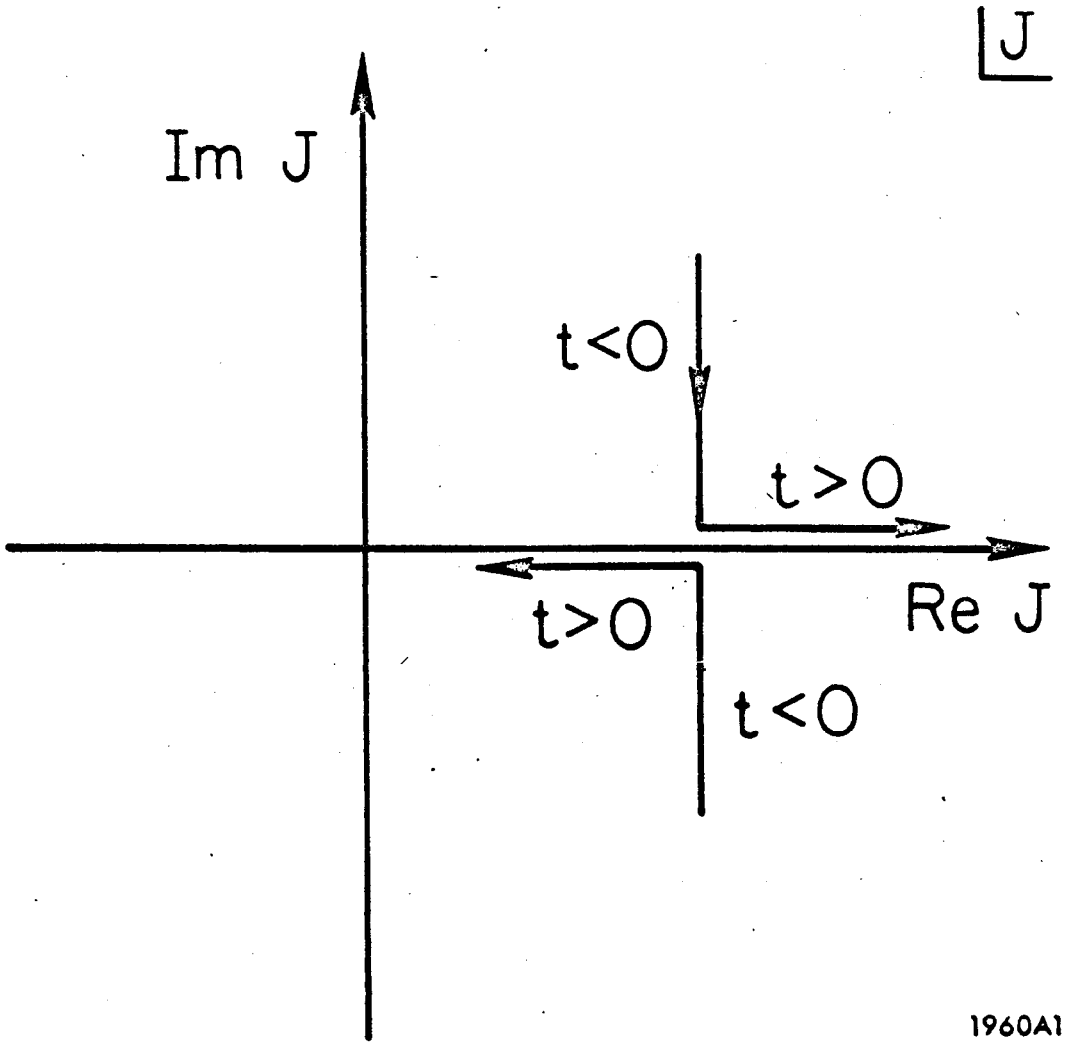

Fig. 8